# Event-Based Intermittent Formation Control of Multi-UAV Systems Under Deception Attacks

Tingting Yin, Zhou Gu, *Member, IEEE*, and Ju H. Park, *Senior Member, IEEE*

***Abstract*— This article investigates the problem of event-based intermittent formation control for multi-UAV systems subject to deception attacks. Compared to the available research studies on multi-UAV systems with continuous control strategy, the proposed intermittent control strategy saves a large amount of computation resources. An average method is introduced in developing the event-triggered mechanism (ETM) such that the amount of unexpected triggering events induced by uncertain disturbances is greatly reduced. Moreover, such a mechanism can further decrease the average data-releasing rate, thereby alleviating the burden of network bandwidth. Sufficient conditions for multi-UAV systems with deception attacks to achieve the predefined formation are obtained with the aid of Lyapunov stability theory. Finally, the validity of the proposed theoretical results is demonstrated via a simulation example.**

***Index Terms*— Event-triggered mechanism (ETM), intermittent formation control, multiagent system, unmanned aerial vehicle (UAV).**

## I. Introduction

OVER the past decades, multiagent systems have received considerable research attention as a result of their widespread applications, for instance, in satellite formation, collaborative load transport of robots, autonomous surface vehicles, unmanned aerial vehicles (UAVs), and so on [1], [2], [3], [4], [5], [6]. It is well known that UAVs can be regarded as a typical representative of agents [7]. Compared to other aerocrafts, UAV systems have plenty of advantages in performing an assigned mission. For example, UAV systems do not require stewards to ensure personal safety, especially in dangerous conditions. However, in most cases, it is hard for a single UAV to complete a complex mission. In this situation, the problem of cooperative formation control for multi-UAV systems has attracted many researchers [8], [9], [10], [11], [12]. Therefore, to complete the task of formation tracking, it is essential to design a suitable control strategy for multi-UAV systems [13], [14], [15]. In recent years, lots of efforts have been devoted to the issue of cooperative formation control of multi-UAV systems [16], [17], [18], [19], [20], and the references therein. For example, Wang et al. [21] focused on the issue of the cooperative moving path following UAV systems with speed constraints. The problem of decentralized overlapping formation control for multi-UAV systems was investigated in [22]. Dong et al. [2] developed a formation control strategy for multi-UAV systems, where the undirected communication topology among follower UAVs was considered. In undirected graphs of multi-UAV systems, bidirectional information interaction of multiple followers consumes more communication and computation resources. Consequently, the directed graph is considered to be more reasonable and practical. Unlike the undirected graph, the Laplacian matrix of directed graphs is asymmetric, which leads to the results of undirected graphs in [2] that cannot be directly applied to directed graphs. Besides, the intermittent control strategy has also attracted increasing attention owing to its advantages in saving the limited computation and energy resources [23], [24], [25], [26]. Therefore, it is a meaningful and challenging task to develop appropriate formation control strategies for multi-UAV systems with directed graphs via an intermittent control method, which is one of the main motivations of this research.

For the multi-UAV system, information interaction among multiple UAVs is necessary for flight formation construction and transformation. The wireless network generally severs as a medium for data communication. Therefore, the efficiency and quality of information interaction among multiple UAVs play an imperative role in improving the performance of multi-UAV systems. To improve the utilization of the limited network resource, time-triggered control is first considered due to its easy implementation. However, such a communication scheme may bring information redundancy, thereby resulting in resource waste and even network congestion. For such a reason, a discrete event-triggered mechanism (ETM) proposed in [27] is extensively employed. Under this scheme, the sampling measurement is transmitted over the network only when the predetermined event-triggering condition is violated. Recent years have witnessed the application and development of discrete ETM [28], [29], [30], [31], [32], [33]. Inspired by such a scheme, some extended communication schemes,

Manuscript received 6 August 2021; revised 29 April 2022, 10 August 2022, and 18 October 2022; accepted 1 December 2022. This work was supported in part by the National Natural Science Foundation of China under Grant 62273183, Grant 62022044, and Grant 62103193; and in part by the Postgraduate Research and Practice Innovation Program of Jiangsu Province, China, under Grant KYCX21_0871. The work of Ju H. Park was supported by the National Research Foundation of Korea (NRF) Grant funded by the Korean Government (Ministry of Science and Information and Communications Technology) under Grant 2019R1A5A8080290. *(Corresponding authors: Zhou Gu; Ju H. Park.)*

Tingting Yin and Zhou Gu are with the College of Mechanical and Electronic Engineering, Nanjing Forestry University, Nanjing 210037, China (e-mail: yttangle@163.com; gzh1808@163.com).

Ju H. Park is with the Department of Electrical Engineering, Yeungnam University, Gyeongsan 38541, South Korea (e-mail: jessie@ynu.ac.kr).

Color versions of one or more figures in this article are available at https://doi.org/10.1109/TNNLS.2022.3227101.

Digital Object Identifier 10.1109/TNNLS.2022.3227101

such as hybrid-triggered scheme [34], adaptive ETM [35] and memory-based ETM [36], [37] spring up. The memory-based ETM was used in [38] to address the problem of secure control for cloud-aided active suspension systems, easing the network bandwidth load. Under the memory-based ETM, both the immediate sampled data and the newest released signals are considered in designing the event-triggering condition. However, it is a challenging issue to design event-triggering conditions by utilizing an average method to further save network capital and ensure the performance of multi-UAV systems. This is another motivation for this study.

Note that the wireless communication network for multi-UAV systems is vulnerable to cyber-attacks. As such, the issue of cyber-security for UAV systems has received considerable attention over the past years. There are three types of cyber-attacks usually discussed in the existing literature: replay attacks, denial-of-service (DoS) attacks, and deception attacks [3]. The deception attacks inject false data into the transmitted signals, thus causing the degradation of the system's performance. Adversaries launch DoS attacks by occupying the limited communication resources to intercept data transmission, crippling the system's functionality. A significant number of results related to cyber-attacks have been acquired [28], [39], [40], [41], and the references therein. For instance, Peng and Sun [40] proposed a switching-like event-triggered control strategy for networked control systems subject to DoS attacks. By considering deception attacks, the security control issue of T-S fuzzy systems with historical information-based ETM was addressed in [37]. The problem of the distributed $H_\infty$-consensus filtering was discussed in [41] for discrete systems considering deception attacks. However, up to now, there are few studies on multi-UAV systems subject to cyber-attacks. The research on the formation control problem of multi-UAV systems under deception attacks is still challenging work.

Based on the above discussion, we mainly focus on the issue of the event-based intermittent formation control of multi-UAV systems with directed graphs in the presence of deception attacks. The main contributions of this study include the following.

1) A new ETM for multi-UAV systems is developed to save the limited communication resources, in which an average method is used to reduce unexpected triggering events aroused by sudden disturbances. Compared with the existing event-triggered schemes in [27] and [29], the proposed communication scheme can further decrease the average data-releasing rate while maintaining the UAV system performance at a prescribed level.
2) A novel intermittent control strategy is proposed for multi-UAV systems with directed graphs and deception attacks. Different from the traditional continuous control that needs to work continuously during the whole sampled interval [2], [20], such an intermittent control only works in some control intervals, thus reducing the consumption of computation and energy resources, and increasing the flight endurance time.

The rest of this study is summarized as follows. The problem formulation and modeling for the discussed multi-UAV system are given in Section II. Section III gives the main results of the event-based intermittent formation control for multi-UAV systems with directed graphs and deception attacks. A simulation example exhibited in Section IV confirms the feasibility of the obtained results. Section V presents the conclusion of this study.

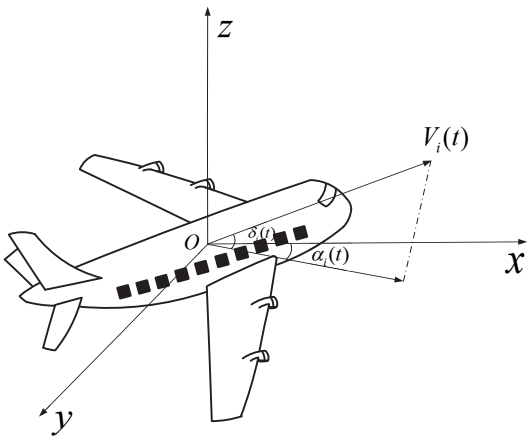


Fig. 1. Diagram of the $i$th UAV.

*Notation:* $\mathbb{R}^n$ denotes the $n$-dimensional Euclidean space. $I_{m\times n}$ and $0_{m\times n}$ are the $m \times n$-dimensional identity (zero) matrix, and sometimes they can be abbreviated as $I$ and 0, respectively. $*$ in a symmetric matrix is the entry implied by symmetry. $\lambda_{\max(\min)}(X)$ is the maximum (minimum) eigenvalue of the matrix $X$.

## II. Problem Description and Modeling

### A. Basic Graph Theory

The communication topology among $N$ UAVs can be described by a directed graph $\mathcal{F} = (\mathbb{V}, \mathbb{E}, \mathbb{W})$, where $\mathbb{E} \subseteq \{(i, j), i, j \in \mathbb{V}\}$ and $\mathbb{V} \in \{1, 2, \ldots, N\}$ indicate the set of edges and nodes, respectively. The weighted adjacency $\mathbb{W} = [w_{ij}]$ of $\mathcal{F}$ is defined as $w_{ii} = 0$, $w_{ij} = 1 \Leftrightarrow (j, i) \in \mathbb{E}$; otherwise, $w_{ij} = 0$. The information of the $i$th UAV can be available to the $j$th UAV, which is described as the edge $(i, j) \in \mathbb{E}$ of $\mathcal{F}$. Define the Laplacian matrix $\mathbb{L} = [\mathscr{L}_{ij}]$, where $\mathscr{L}_{ii} = \Sigma_{j\neq i} w_{ij}$, and $\mathscr{L}_{ij} = -w_{ij}$ for $i \neq j$, $i, j \in \mathbb{V}$. Denote $\mathbb{S}_i = \{j|(i, j) \in \mathbb{E}\}$ as the set containing all neighbors of the $i$th UAV.

*Remark 1:* In an undirected graph, edge $(i, j) \in \mathbb{E}$ denotes bidirectional information interaction between the $i$th UAV and the $j$th UAV, thereby consuming quantities of communication and computation resources. To reduce unnecessary waste of limited resources, the directed topology graph is considered in this research on the issue of the event-based formation control of multi-UAV systems.

### B. Dynamical Model of UAVs

Consider a class of multi-UAV systems that contains one virtual leader (labeled as the 0th UAV) and $N$ following UAVs (labeled as $1, 2, \ldots, N$). The kinematic equation of the $i$th

fixed-wing UAV is expressed as follows [15], [42]:

$$\begin{cases} \dot{\zeta}_{xi}(t) = V_i(t)\cos\delta_i(t)\cos\alpha_i(t) \\ \dot{\zeta}_{yi}(t) = V_i(t)\cos\delta_i(t)\sin\alpha_i(t) \\ \dot{\zeta}_{zi}(t) = V_i(t)\sin\delta_i(t) \end{cases} \tag{1}$$

where $\zeta_i(t) = [\zeta_{xi}(t)\ \zeta_{yi}(t)\ \zeta_{zi}(t)]^T$ is the position of the $i$th UAV. As shown in Fig. 1, $\delta_i(t)$ $[\alpha_i(t)]$ denotes the $i$th UAV's flight path bank (azimuth) angle, $\cos(\delta_i(t)) \neq 0$. $V_i(t) > 0$ $(i = 0, 1, 2, \ldots, N)$ represents the flight speed. For the $i$th follower UAV $(i = \{1, 2, \ldots, N\} \triangleq \mathcal{G})$, the following equations are satisfied:

$$\begin{cases} \dot{V}_i(t) = a_{xi} - g\sin\delta_i(t) \\ \dot{\alpha}_i(t) = \dfrac{a_{yi}}{V_i(t)\cos\delta_i(t)} \\ \dot{\delta}_i(t) = \dfrac{a_{zi}}{V_i(t)} - \dfrac{g\cos\delta_i(t)}{V_i(t)} \end{cases} \tag{2}$$

where $g$ indicates the acceleration of gravity; $a_{xi}$, $a_{yi}$, and $a_{zi}$ stand for the acceleration of roll, pitch, and yaw, respectively. Then, we can obtain the real control $\hbar_i(t) = [a_{xi}\ a_{yi}\ a_{zi}]^T$. For convenience, $\delta_i(t)$ and $\alpha_i(t)$ are abbreviated as $\delta_i$ and $\alpha_i$ in the following, respectively.

Deriving the equalities in (1) and substituting $\dot{V}_i(t)$, $\dot{\alpha}_i(t)$ and $\dot{\delta}_i(t)$ in (2) into them yield that

$$\ddot{\zeta}_i(t) = \jmath_i(t)\hbar_i(t) + \begin{bmatrix} 0 & 0 & -g \end{bmatrix}^T \tag{3}$$

where

$$\jmath_i(t) = \begin{bmatrix} \cos\delta_i\cos\alpha_i & -\sin\alpha_i & -\sin\delta_i\cos\alpha_i \\ \cos\delta_i\sin\alpha_i & \cos\alpha_i & -\sin\delta_i\sin\alpha_i \\ \sin\delta_i & 0 & \cos\delta_i \end{bmatrix}.$$

Denote $\upsilon_i(t) = \dot{\zeta}_i(t)$ as the velocity vector of the $i$th UAV, and $u_i(t) = \jmath_i(t)\hbar_i(t) + [0\ 0\ -g]^T$ as a new control input, then, it is easy to obtain that $\dot{\zeta}_i(t) = \upsilon_i(t)$ and $\dot{\upsilon}_i(t) = u_i(t)$. In this study, deception attacks are taken into consideration. Then, the following state of the $i$th UAV under deception attacks is considered:

$$\begin{cases} \dot{\zeta}_i(t) = \upsilon_i(t) \\ \dot{\upsilon}_i(t) = u_i(t) + E_0 f_i(t) \end{cases} \tag{4}$$

where $f_i(t)$ denotes the deception attack signal; $E_0$ is a known constant matrix with appropriate dimensions.

Defining $x_i(t) = \begin{bmatrix} \zeta_i(t) \\ \upsilon_i(t) \end{bmatrix}$, $A = \begin{bmatrix} 0 & I_3 \\ 0 & 0 \end{bmatrix}$, $B = \begin{bmatrix} 0 \\ I_3 \end{bmatrix}$, $E = \begin{bmatrix} 0 \\ E_0 \end{bmatrix}$, one has

$$\begin{cases} \dot{x}_i(t) = Ax_i(t) + Bu_i(t) + Ef_i(t) \\ y_i(t) = C_1 x_i(t) \end{cases} \tag{5}$$

where $y_i(t)$ denotes the system output; $C_1$ is a constant matrix.

*Assumption 1:* The directed communication topology $\mathcal{F}$ of the multi-UAV system has a directed spanning tree, and the root node is the virtual leader UAV.

*Remark 2:* According to Assumption 1, the connectivity of information interaction between two arbitrary UAVs can be guaranteed in the directed topology graph, which is significant to design the following formation controller in this research.

In this study, it is assumed that the formation trajectory of each UAV is predefined. To obtain the trajectory of the $i$th UAV, now we first describe the relative position between the $i$th UAV and the 0th UAV. Similar to [20] and [42], we define the following characters for the $i$th UAV: $\chi_i(t)$, satisfying $-(\pi/2) \leq \chi_i(t) \leq (\pi/2)$, is the acute angle between the connecting line (it links the $i$th UAV and the 0th UAV) and the $xy$ plane; $\beta_i(t)$ is the included angle between the projection of the distance $s_i$ and relative velocity $d_{vi}(t)$ on the $xy$ plane, wherein $s_i$ stands for the distance between the $i$th UAV and the 0th UAV. Denote the desired relative position as $\Delta\zeta_i(t) = [\Delta\zeta_{xi}(t)\ \Delta\zeta_{yi}(t)\ \Delta\zeta_{zi}(t)]^T$, where

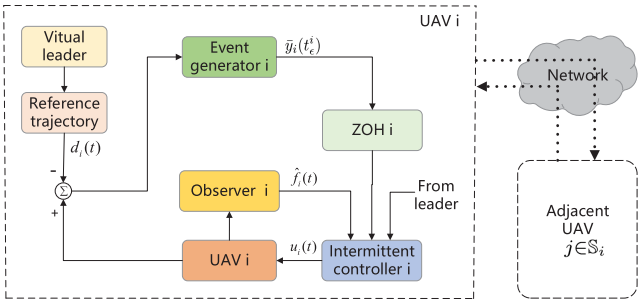


Fig. 2. Block diagram of event-based intermittent formation control for the $i$th UAV.

$$\begin{cases} \Delta\zeta_{xi}(t) = -s_i\cos(\chi_i + \delta_0)\cos(\beta_i + \alpha_0) \\ \Delta\zeta_{yi}(t) = -s_i\cos(\chi_i + \delta_0)\sin(\beta_i + \alpha_0) \\ \Delta\zeta_{zi}(t) = -s_i\sin(\chi_i + \delta_0) \end{cases} \tag{6}$$

in which $\chi_i$ and $\beta_i$ are the abbreviation of $\chi_i(t)$ and $\beta_i(t)$, respectively. Moreover, the desired position of the $i$th UAV can be expressed by $d_{\zeta i}(t) = \zeta_0(t) + \Delta\zeta_i(t)$, where $\zeta_0(t) = [\zeta_{x0}(t)\ \zeta_{y0}(t)\ \zeta_{z0}(t)]^T$ is the position of the 0th UAV. Then, denote the tracking error for the $i$th UAV as $\bar{x}_i(t) = x_i(t) - d_i(t)$, where $d_i(t) = [d_{\zeta i}^T(t)\ d_{vi}^T(t)]^T$, $d_{vi}(t) = \dot{d}_{\zeta i}(t)$.

*Remark 3:* To achieve the $i$th UAV formation trajectory, we perform the following steps. First, obtain $d_i(t)$ based on (6). Note that the desired relative state $d_i(t)$ between the $i$th UAV and the 0th UAV includes the relative position $d_{\zeta i}(t)$ and the relative velocity $d_{vi}(t)$; Second, describe the tracking error $\bar{x}_i(t)$.

Fig. 2 presents the block diagram of the formation control for the $i$th UAV, from which one can see that the controller $i$ receives the information of the leader UAV, the $i$th UAV, and its adjacent UAVs. Deception attacks are considered due to the data transmission via the network. Observer $i$ is used to observe the attack signal $f_i(t)$. The zero-order hold (ZOH) is introduced to keep the latest input of intermittent controller $i$ until the next signal arrives.

### C. Attack Observer-Based Intermittent Control Strategy

Deception attacks are considered in each UAV in this study. To estimate and eliminate the impacts of the deception attack for every UAV, the attack observer for the $i$th UAV is designed as follows:

$$\begin{cases} \dot{\xi}_i(t) = HC_1E[C_2\xi_i(t) + C_2Hy_i(t)] - HC_1[Ax_i(t) + Bu_i(t)] \\ \hat{f}_i(t) = -C_2Hy_i(t) - C_2\xi_i(t) \end{cases} \tag{7}$$

where $\xi_i(t)$ is the intermediate variable; $\hat{f}_i(t)$ denotes the estimated deception attack signal. $H$ represents the observer gain to be determined. $C_2$ is an invertible parameter matrix with appropriate dimensions.

To reduce the consumption of computation and energy resources for multi-UAV systems, we construct a periodically intermittent control $u_c^i(t)$. As stated in [23] and [43], the control time is denoted by $[n\mathcal{T}, n\mathcal{T}+\varsigma)$ and the rest time by $[n\mathcal{T}+\varsigma, (n+1)\mathcal{T})$, where $\varsigma \in (0, \mathcal{T}]$ is the control duration in a period $\mathcal{T}$. Then, we propose the following control strategy for multi-UAV systems under directed topology graphs:

$$u_i(t) = u_c^i(t) - B^+ E\hat{f}_i(t) + \dot{d}_{vi}(t) \tag{8}$$

where

$$u_c^i(t) = \begin{cases} u_k^i(t), & t \in [n\mathcal{T}, n\mathcal{T}+\varsigma) \\ 0, & t \in [n\mathcal{T}+\varsigma, (n+1)\mathcal{T}) \end{cases}$$

$$u_k^i(t) = -K\left\{\sum_{j\in\mathbb{S}_i} w_{ij}[\bar{y}_i(t_\epsilon^i) - \bar{y}_j(t_{\epsilon'}^j)] + b_i\bar{y}_i(t_\epsilon^i)\right\}$$

for $n \in \mathcal{N}$, $\mathcal{N}$ is the set of nonnegative integers. $\bar{y}_i(t_\epsilon^i)$ represents the event-triggered signal, and $\bar{y}_i(t_\epsilon^i) = C_1\bar{x}_i(t_\epsilon^i)$. $\bar{y}_j(t_{\epsilon'}^j)$ denotes the latest transmitted signal from the $j$th UAV, where $\epsilon' \triangleq \operatorname{argmin}_{\epsilon'}\{t - t_{\epsilon'}^j | t > t_{\epsilon'}^j, \epsilon' = 0, 1, 2, 3, \ldots\}$; $\dot{d}_{vi}(t)$ denotes the desired acceleration; and $K$ denotes the controller gain to be determined. The matrix $B^+$ satisfies $(I - BB^+)E = 0$.

*Remark 4:* In (8), the intermittent control $u_c^i(t)$ belongs to a periodic control strategy and each control period contains the control time and the rest time.

*Remark 5:* Compared to the traditional continuous controller, the intermittent controller $u_c^i(t)$ in (8) only works in control intervals $\bigcup_{n\in\mathcal{N}}[n\mathcal{T}, n\mathcal{T}+\varsigma)$. In other words, it is not working in the rest time $\bigcup_{n\in\mathcal{N}}[n\mathcal{T}+\varsigma, (n+1)\mathcal{T})$, thereby saving limited computing and energy resources. Especially, if one sets $\varsigma = \mathcal{T}$, the intermittent controller $u_c^i(t)$ becomes a traditional continuous controller as in [2] and [20].

### D. ETMs Using an Average Method

To save the resources of the UAV communication network, the ETM using an average method is developed, which is shown in Fig. 2. Whether the system output of the $i$th UAV should be transmitted or not is decided by the following triggering condition:

$$e_{yi}^T(t)\Phi_i e_{yi}(t) \le \sigma_i(t)\varpi_{yi}^T(t)\Phi_i\varpi_{yi}(t) \tag{9}$$

where

$$\begin{aligned} \varpi_{yi}(t) &= \sum_{j\in\mathbb{S}_i} w_{ij}[\vartheta_{yi}(t) - \vartheta_{yj}(t)] \\ \vartheta_{yi}(t) &= \frac{1}{2}\left[\bar{y}_i(t_\epsilon^i) + \bar{y}_i(t)\right] \\ e_{yi}(t) &= \vartheta_{yi}(t) - \bar{y}_i(t) \\ &= C_1 \cdot \frac{1}{2}\left[\bar{x}_i(t_\epsilon^i) - \bar{x}_i(t)\right] \triangleq C_1 e_i(t) \end{aligned}$$

in which $\sigma_i(t) = \underline{\sigma}_i + (2/\pi)(\bar{\sigma}_i - \underline{\sigma}_i)\arctan(\| \varpi_{yi}(t) \|)$, $\sigma_i(t) \in [\underline{\sigma}_i, \bar{\sigma}_i)$, $\underline{\sigma}_i, \bar{\sigma}_i \in [0, 1)$; $\Phi_i > 0$ is the weight matrix. Here the event-triggered instants of the $i$th UAV are denoted as $\{t_0^i, t_1^i, \ldots, t_\epsilon^i, \ldots\}$, which satisfy $t_0^i = 0$ and $t_0^i < t_1^i < \cdots < t_\epsilon^i < \cdots$, where $\epsilon \in \{0, 1, 2, \ldots\}$, $i \in \mathcal{G}$. The leader UAV does not concern with the triggering issue in this study.

Then, the event-triggered signal $\bar{y}_i(t_\epsilon^i)$ can be expressed as

$$\bar{y}_i(t_\epsilon^i) = \bar{y}_i(t) + 2e_{yi}(t). \tag{10}$$

*Remark 6:* From (9), one can see that an average $\vartheta_{yi}(t)$ of the system output signal $\bar{y}_i(t)$ and the latest triggering signal $\bar{y}_i(t_\epsilon^i)$ is utilized for the proposed ETM. This would bring many advantages, for example, it can mitigate the unexpected triggering event caused by the accidentally sudden state variation, and smooth the releasing period.

*Remark 7:* Differentiating from the existing research on multi-UAV formation control, the dynamic ETM using the average method is developed, and the threshold $\sigma_i(t)$ can be adaptively adjusted according to the real-time information of UAVs. Under such an ETM, the system output signal $\bar{y}_i(t)$ is transmitted through the network only when it violates inequality (9), thus greatly reducing redundant data and relieving network bandwidth burden.

Let the estimation error $\eta_f^i(t) = f_i(t) - \hat{f}_i(t)$, then, combining (5), (7), (8), and (10) and using the Kronecker product yield that

$$\dot{\eta}_f(t) = \dot{f}(t) + \bar{C}_2\bar{H}\bar{C}_1\bar{E}\eta_f(t) \tag{11}$$

and

$$\dot{\bar{x}}(t) = \begin{cases} \vartheta_x(t), & t \in \bigcup\limits_{n\in\mathcal{N}}[n\mathcal{T}, n\mathcal{T}+\varsigma) \\ \bar{A}\bar{x}(t) + \bar{E}\eta_f(t), & t \in \bigcup\limits_{n\in\mathcal{N}}[n\mathcal{T}+\varsigma, (n+1)\mathcal{T}) \end{cases} \tag{12}$$

where

$$\vartheta_x(t) = (\bar{A} - L_1\bar{B}\bar{K}\bar{C}_1)\bar{x}(t) - 2L_1\bar{B}\bar{K}\bar{C}_1 e(t) + \bar{E}\eta_f(t)$$

with $\bar{A} = I_N \otimes A$, $\bar{B} = I_N \otimes B$, $\bar{E} = I_N \otimes E$, $\bar{H} = I_N \otimes H$, $\bar{C}_1 = I_N \otimes C_1$, $\bar{C}_2 = I_N \otimes C_2$, $L_1 = L_0 \otimes I_6$, $L_0 = \mathbb{L} + B_0$, $B_0 = \operatorname{diag}\{b_1, b_2, \ldots, b_N\}$ and $\bar{x}(t) = [\bar{x}_1^T(t), \bar{x}_2^T(t), \ldots, \bar{x}_N^T(t)]^T$, $e(t) = [e_1^T(t), e_2^T(t), \ldots, e_N^T(t)]^T$, $\eta_f(t) = [(\eta_f^1)^T(t), (\eta_f^2)^T(t), \ldots, (\eta_f^N)^T(t)]^T$, $\dot{f}(t) = [\dot{f}_1^T(t), \dot{f}_2^T(t), \ldots, \dot{f}_N^T(t)]^T$.

Defining $\eta(t) = \begin{bmatrix} \bar{x}(t) \\ \eta_f(t) \end{bmatrix}$ yields the following error system:

$$\begin{cases} \dot{\eta}(t) = \mathcal{A}^\iota\eta(t) + \mathcal{B}^\iota e(t) + \mathcal{E}^\iota\eta_f(t) \\ z(t) = \bar{D}G\eta(t) \end{cases} \tag{13}$$

where $\iota = 1, 2$; when $t \in \bigcup_{n\in\mathcal{N}}[n\mathcal{T}, n\mathcal{T}+\varsigma)$, $\iota = 1$; when $t \in \bigcup_{n\in\mathcal{N}}[n\mathcal{T}+\varsigma, (n+1)\mathcal{T})$, $\iota = 2$; and $\mathcal{A}^1 = \mathcal{A}_1$, $\mathcal{A}^2 = \mathcal{A}_2$, $\mathcal{B}^1 = \mathcal{B}$, $\mathcal{B}^2 = 0$, $\mathcal{E}^1 = \mathcal{E}^2 = \mathcal{E}$; $z(t)$ is the output of the multi-UAV system; $\bar{D} = I_N \otimes D$, $D$ is a known matrix with suitable dimensions; $G = [I_{6N}\ 0_{6N\times 3N}]$ and

$$\mathcal{A}_1 = \begin{bmatrix} \bar{A} - L_1\bar{B}\bar{K}\bar{C}_1 & \bar{E} \\ 0 & \bar{C}_2\bar{H}\bar{C}_1\bar{E} \end{bmatrix}, \quad \mathcal{A}_2 = \begin{bmatrix} \bar{A} & \bar{E} \\ 0 & \bar{C}_2\bar{H}\bar{C}_1\bar{E} \end{bmatrix}$$

$$\mathcal{B} = \begin{bmatrix} -2L_1\bar{B}\bar{K}\bar{C}_1 \\ 0 \end{bmatrix}, \quad \mathcal{E} = \begin{bmatrix} 0_{6N\times 3N} \\ I_{3N} \end{bmatrix}.$$

This study aims to propose an intermittent control strategy for multi-UAV systems with directed graphs and deception attacks to achieve the formation by applying the proposed ETM such that the discussed error system is asymptotically stable.

## III. Main Results

The stability analysis of the event-based formation control of multiple UAVs with directed topology graphs and deception attacks via an intermittent control method will be presented in this section. The following assumption is introduced to facilitate the proof procedures before showing the main results.

*Definition 1:* The error system (13) with the event-triggered control strategy (8) is exponentially stable if there exists a scalar $\upsilon > 0$ and a decay rate $\omega$ such that

$$\|\eta(t)\| \leq \upsilon e^{-\omega t}\|\eta_0\|$$

for all $t \geq 0$. $\eta_0 = \eta(0)$.

*Remark 8:* Note that $\eta(t)$ contains the tracking error $\bar{x}(t)$ and the attack estimation error $\eta_f(t)$ here. When the error system (13) is asymptotically stable, $\bar{x}(t) \to 0$ and $\eta_f(t) \to 0$, which implies that the multi-UAV system can realize the desired formation according to Definition 1.

*Theorem 1:* For given scalars $\mathcal{T}$, $\varsigma$, $\bar{\sigma}_i \in (0,1)$, $\varrho_\iota$ ($\iota = \{1,2\}$), controller gain $K$ and observer gain $H$, the error system in (13) is exponentially stable if there exist matrices $\bar{P} > 0$, $\Phi_i > 0$ ($i \in \mathcal{G}$) such that

$$\Upsilon_1 = \begin{bmatrix} \Xi_{11}^1 & * & * \\ \Xi_{21}^1 & \Xi_{22}^1 & * \\ \mathcal{E}^T\bar{P} & 0 & -\gamma^2 I \end{bmatrix} < 0 \tag{14}$$

$$\Upsilon_2 = \begin{bmatrix} \Xi_{11}^2 & * \\ \mathcal{E}^T\bar{P} & -\gamma^2 I \end{bmatrix} < 0 \tag{15}$$

$$\kappa = \varrho_1\varsigma - \varrho_2(\mathcal{T}-\varsigma) > 0 \tag{16}$$

where

$$\begin{aligned}
\Xi_{11}^\iota &= \bar{P}\mathcal{A}_1 + \mathcal{A}_1^T\bar{P} + G^T\bar{C}_1^T L_2^T\bar{\sigma}\Phi L_2\bar{C}_1 G \\
&\quad + \varrho_1\bar{P} + G^T\bar{D}^T\bar{D}G \\
\Xi_{21}^1 &= \mathcal{B}_1^T\bar{P} + \frac{1}{2}G^T\bar{C}_1^T L_2^T\bar{\sigma}\Phi L_2\bar{C}_1 G \\
\Xi_{22}^1 &= -\bar{C}_1^T\Phi\bar{C}_1 + \frac{1}{4}\bar{C}_1^T L_2^T\bar{\sigma}\Phi L_2\bar{C}_1 \\
\Xi_{11}^2 &= \bar{P}\mathcal{A}_2 + \mathcal{A}_2^T\bar{P} - \varrho_2\bar{P} + G^T\bar{D}^T\bar{D}G \\
\bar{\sigma} &= \hat{\sigma}\otimes I_6, \hat{\sigma} = \mathrm{diag}\{\bar{\sigma}_1, \bar{\sigma}_2, \ldots, \bar{\sigma}_N\} \\
\Phi &= \mathrm{diag}\{\Phi_1, \Phi_2, \ldots, \Phi_N\}.
\end{aligned}$$

*Proof:* The whole proof process is mainly compartmentalized into two steps. The stability analysis of system (13) is presented in Step I, and the discussion on the exclusion of the Zeno behavior is given in Step II.

*Step I:* Choose the following Lyapunov function for system (13):

$$V(\eta(t)) = \eta^T(t)\bar{P}\eta(t). \tag{17}$$

It follows that:

$$\lambda_{\min}(\bar{P})\|\eta(t)\|^2 \leq V(\eta(t)) \leq \lambda_{\max}(\bar{P})\|\eta(t)\|^2 \tag{18}$$

where $\bar{P} = \mathrm{diag}\{\bar{P}_1, \bar{P}_2\}$, $\bar{P}_1 = I_N \otimes P_1$, $\bar{P}_2 = I_N \otimes P_2$.

In the following, two situations are considered for $t \in \bigcup_{n\in\mathcal{N}}[n\mathcal{T}, n\mathcal{T}+\varsigma)$ and $t \in \bigcup_{n\in\mathcal{N}}[n\mathcal{T}+\varsigma, (n+1)\mathcal{T})$, respectively.

First of all, when $t \in \bigcup_{n\in\mathcal{N}}[n\mathcal{T}, n\mathcal{T}+\varsigma)$, calculating the derivation of (17) yields that

$$\begin{aligned}
\dot{V}(\eta(t)) &= 2\eta^T(t)\bar{P}\dot{\eta}(t) \\
&= -\varrho_1 V(\eta(t)) + \eta^T(t)[2\bar{P}\dot{\eta}(t) + \varrho_1\bar{P}\eta(t)] \\
&= -\varrho_1 V(\eta(t)) \\
&\quad + \eta^T(t)\{\varrho_1\bar{P}\eta(t) + 2\bar{P}[\mathcal{A}_1\eta(t) + \mathcal{B}_1 e(t) + \mathcal{E}\eta_f(t)]\}.
\end{aligned} \tag{19}$$

Considering the fact $\arctan(\| \varpi_{yi}(t) \|) \in [0, (\pi/2))$ for $t \geq 0$, we have $\sigma_i(t) < \bar{\sigma}_i$, then, it follows from (9) that:

$$\varpi_x^T(t)\bar{\sigma}\Phi\varpi_x(t) - e^T(t)\bar{C}_1^T\Phi\bar{C}_1 e(t) > 0 \tag{20}$$

where $\varpi_x(t) = L_2\bar{C}_1[G\eta(t) + e(t)]$, $L_2 = L \otimes I_6$.

Combining (19) and (20) and applying the Schur complement yield that

$$\begin{aligned}
&\dot{V}(\eta(t)) + z^T(t)z(t) - \gamma^2\dot{f}^T(t)\dot{f}(t) \\
&\qquad \leq -\varrho_1 V(t) + \varpi_1^T(t)\Upsilon_1\varpi_1(t)
\end{aligned}$$

where $\varpi_1(t) = [\eta^T(t) \;\; e^T(t) \;\; \dot{f}^T(t)]^T$. According to (14), one can obtain that

$$\dot{V}(\eta(t)) + \varrho_1 V(t) - \gamma^2\dot{f}^T(t)\dot{f}(t) + z^T(t)z(t) \leq 0 \tag{21}$$

for $t \in \bigcup_{n\in\mathcal{N}}[n\mathcal{T}, n\mathcal{T}+\varsigma)$.

For $t \in \bigcup_{n\in\mathcal{N}}[n\mathcal{T}+\varsigma, (n+1)\mathcal{T})$, utilizing the similar method yields that

$$\dot{V}(\eta(t)) - \varrho_2 V(t) - \gamma^2\dot{f}^T(t)\dot{f}(t) + z^T(t)z(t) \leq 0 \tag{22}$$

holds.

First, we consider the case that $\dot{f}(t) = 0$, then, it follows from (21) and (22) that the following holds.

1) For $t \in [0, \varsigma)$

$$\begin{aligned}
V(\eta(t)) &\leq V(\eta_0)e^{-\varrho_1 t} \\
V(\eta(\varsigma)) &\leq V(\eta_0)e^{-\varrho_1\varsigma}.
\end{aligned}$$

2) For $t \in [\varsigma, \mathcal{T})$

$$\begin{aligned}
V(\eta(t)) &\leq V(\eta_0)e^{\varrho_2(t-\varsigma))} \\
&\leq V(\eta_0)e^{-\varrho_1\varsigma+\varrho_2(t-\varsigma)} \\
V(\eta(\mathcal{T})) &\leq V(\eta_0)e^{-\varrho_1\varsigma+\varrho_2(t-\varsigma)}.
\end{aligned}$$

3) For $t \in [\mathcal{T}, \mathcal{T}+\varsigma)$

$$\begin{aligned}
V(\eta(t)) &\leq V(\eta(\mathcal{T}))e^{-\varrho_1(t-\mathcal{T})} \\
&\leq V(\eta_0)e^{-\varrho_1\varsigma-\varrho_1(t-\mathcal{T})+\varrho_2(\mathcal{T}-\varsigma)} \\
V(\eta(\mathcal{T}+\varsigma)) &\leq V(\eta_0)e^{-2\varrho_1\varsigma+\varrho_2(\mathcal{T}-\varsigma)}.
\end{aligned}$$

4) For $t \in [\mathcal{T}+\varsigma, 2\mathcal{T})$

$$\begin{aligned}
V(\eta(t)) &\leq V(\eta(\mathcal{T}+\varsigma))e^{\varrho_2(t-\mathcal{T}-\varsigma)} \\
&\leq V(\eta_0)e^{-2\varrho_1\varsigma+\varrho_2(\mathcal{T}-\varsigma)+\varrho_2(t-\mathcal{T}-\varsigma)} \\
V(\eta(2\mathcal{T})) &\leq V(\eta_0)e^{-2\varrho_1\varsigma+2\varrho_2(\mathcal{T}-\varsigma)}.
\end{aligned}$$

By induction, it yields that

5) For $t \in [n\mathcal{T}, n\mathcal{T}+\varsigma)$, that is, $t-\varsigma/\mathcal{T} < n \leq t/\mathcal{T}$, then, it can be acquired that

$$\begin{aligned} V(\eta(t)) &\leq V(\eta(n\mathcal{T}))e^{-\varrho_1(t-n\mathcal{T})} \\ &\leq V(\eta_0)e^{-n\varrho_1\varsigma+n\varrho_2(\mathcal{T}-\varsigma)} \\ &\leq V(\eta_0)e^{-\frac{\varrho_1\varsigma-\varrho_2(\mathcal{T}-\varsigma)}{\mathcal{T}}\cdot(t-\varsigma)}. \end{aligned} \tag{23}$$

6) For $t \in [n\mathcal{T}+\varsigma, (n+1)\mathcal{T})$, that is, $\varsigma/\mathcal{T} < n+1 \leq t+\mathcal{T}-\varsigma/\mathcal{T}$, then, we have

$$\begin{aligned} V(\eta(t)) &\leq V(\eta(n\mathcal{T}+\varsigma))e^{\varrho_2(t-n\mathcal{T}-\varsigma)} \\ &\leq V(\eta_0)e^{-(n+1)\varrho_1\varsigma+(n+1)\varrho_2(\mathcal{T}-\varsigma)} \\ &\leq V(\eta_0)e^{-\frac{\varrho_1\varsigma-\varrho_2(\mathcal{T}-\varsigma)}{\mathcal{T}}\cdot t} \\ &\leq V(\eta_0)e^{-\frac{\varrho_1\varsigma-\varrho_2(\mathcal{T}-\varsigma)}{\mathcal{T}}\cdot(t-\varsigma)}. \end{aligned} \tag{24}$$

Based on (23) and (24), we can obtain that

$$V(\eta(t)) \leq V(\eta_0)e^{-\frac{\varrho_1\varsigma-\varrho_2(\mathcal{T}-\varsigma)}{\mathcal{T}}\cdot(t-\varsigma)}. \tag{25}$$

Combining (18) and (25) yields that

$$\| \eta(t) \| \leq \mathcal{R}e^{-\omega t} \| \eta_0 \| \quad \forall t \geq 0 \tag{26}$$

where $\mathcal{R} = ((\lambda_{\max}/\lambda_{\min}))^{1/2}e^{(\varsigma/\mathcal{T})}$, $\omega = (\kappa/\mathcal{T})$, $\kappa = \varrho_1\varsigma - \varrho_2(\mathcal{T}-\varsigma)$. This implies that system (13) is exponentially stable.

Second, in the case of $\dot{f}(t) \neq 0$, integrating (21) and (22) from $n\mathcal{T}$ to $(n+1)\mathcal{T}$ follows that:

$$\begin{aligned} \sum_{k=0}^{n}\int_{k\mathcal{T}}^{(k+1)\mathcal{T}} \big[\dot{V}(t) &+ (-1)^{\iota+1}\varrho_\iota V(t) \\ &-\gamma^2\dot{f}^T(t)\dot{f}(t) + z^T(t)z(t)\big]dt \leq 0. \end{aligned} \tag{27}$$

Letting $n \to \infty$ yields

$$\int_0^\infty \|z(t)\|^2 \leq \gamma^2\int_0^\infty \|\dot{f}(t)\|^2.$$

Based on the above analysis and discussion, we can conclude that the error system (13) can reach exponential stability if inequalities (14)–(16) hold. That ends the proof.

*Step II:* The exclusion of Zeno behavior in the ETM will be discussed in the form of two cases.

*Case A:* When system (13) approaches stable, $\bar{x}_i(t) = 0$ and $\bar{y}_i(t) = C_1\bar{x}_i(t) = 0$. Denote $\bar{y}(t) = [\bar{y}_1^T(t), \bar{y}_2^T(t), \ldots, \bar{y}_N^T(t)]^T$, then, one has $\bar{y}(t) = 0$. In this situation, (9) is violated and $\bar{y}_i(t)$ will be delivered via the network. It is the last triggering behavior because both the left and right sides of inequality (9) are equal to zero. It indicates that the ETM does not work anymore when the system is stable, which deservedly excludes the Zeno behavior.

*Case B:* Consider the case that $\bar{x}_i(t) \neq 0$, $\bar{y}_i(t) \neq 0$, and $\bar{y}(t) \neq 0$. Motivated by the work in [20], [44], and [45], the following analysis and discussion will be presented to demonstrate that the Zeno behavior is excluded.

Assumed that Zeno behavior occurs at the time interval $\{t^i_{\epsilon+1} - t^i_\epsilon\}$ of the $i$th UAV, in this situation, there has been a finite time $\mathbb{T}_i$ such that inequality $t^i_\epsilon \leq \mathbb{T}_i$ is satisfied for $\mu \in \{1, 2, 3, \ldots\}$, $\lim_{\mu\to\infty} t^i_\epsilon = \mathbb{T}_i$. Based on the definition of limits of sequences, if one gives $\upsilon_i > 0$, there exists an integer $\mathbb{N}_i > 0$ so as to satisfy inequality $\mathbb{T}_i - \upsilon_i < t^i_\epsilon \leq \mathbb{T}_i$ with $i \geq \mathbb{N}_i$ $(i, \mathbb{N}_i \in \{1, 2, 3, \ldots\})$.

Denote $\kappa = \arg\max_i \| e_{yi}(t) \|$, $i \in \mathcal{G}$. From $\| e_{yi}(t) \| \leq \| e_{yi}(t) \|$, one can get $((\| e_{y\kappa}(t) \|)/(\| \bar{y}_\kappa(t) \|)) \leq ((\sqrt{N} \| e_y(t) \|)/(\| \bar{y}(t) \|))$. Once the ETM works, we have $e_{yi}(t) = 0$.

It follows from the term in (9) that $\lambda_{\max}(\Phi_i) \| e_y(t) \|^2 \leq \lambda_{\max}(\Phi_i)\bar{\sigma}_i \| \varpi_{yi}(t) \|^2$, $\varpi_{yi}(t) = \sum_{j\in\mathbb{S}_i} w_{ij}[\vartheta_{yi}(t) - \vartheta_{yj}(t)]$, $\vartheta_{yi}(t) = (1/2)[\bar{y}_i(t^i_\epsilon) + \bar{y}_i(t)]$; $\triangle t_\kappa$ is denoted as the time under which $((\| e_{y\kappa}(t) \|)/(\| \bar{y}_\kappa(t) \|))$ grows from zero to $\bar{\sigma}_i$ $(\bar{\sigma}_i \in (0, 1))$.

Based on the stability proof above, one can see that $e_y(t)$ is bounded. Note that the switched system (12) and the definition of $e_{yi}(t) = (1/2)[\bar{y}_i(t^i_\epsilon) - \bar{y}_i(t)]$, for any certain instant $t^i_\epsilon$, $\dot{\bar{y}}_i(t^i_\epsilon) = 0$, $\dot{e}_{yi}(t) = -(1/2)\dot{\bar{y}}_i(t)$. Two situations are analyzed in the following. When $t \in \bigcup_{n\in\mathcal{N}}[n\mathcal{T}, n\mathcal{T}+\varsigma)$, one has

$$\begin{aligned} \frac{d}{dt}\frac{\| e_y(t) \|}{\| \bar{y}(t) \|} &= -\frac{e_y^T(t)\dot{\bar{y}}(t)}{2\| e_y(t) \|\| \bar{y}(t) \|} - \frac{e_y(t)\bar{y}^T(t)\dot{\bar{y}}(t)}{2\| \bar{y}(t) \|^2\| \bar{y}(t) \|} \\ &\leq \frac{\| e_y^T(t) \|\| \dot{\bar{y}}(t) \|}{\| e_y(t) \|\| \bar{y}(t) \|} + \frac{\| e_y(t) \|\| \bar{y}^T(t) \|\| \dot{\bar{y}}(t) \|}{\| \bar{y}(t) \|^2\| \bar{y}(t) \|} \\ &= \left(1 + \frac{\| e_y(t) \|}{\| \bar{y}(t) \|}\right)\frac{\| \dot{\bar{y}}(t) \|}{\| \bar{y}(t) \|} \\ &\leq (1+\nu)\big(\| \mathcal{H}_1 \| + \| \mathcal{H}_2 \| \nu + \vartheta_{\sup}\big) \end{aligned} \tag{28}$$

where $\nu = ((\| e_y(t) \|)/(\| \bar{y}(t) \|))$, $\mathcal{H}_1 = \bar{A} - L_1\bar{B}\bar{K}$, $\mathcal{H}_2 = -2L_1\bar{B}\bar{K}$; $\vartheta_{\sup}$ is defined as $\vartheta_{\sup} = \sup\{((\| \bar{E}\eta_y(t) \|)/(\| \bar{y}(t) \|))\}$ $(\| \bar{y}(t) \| \neq 0)$.

It follows from the definition of $\nu$ that (28) is repressed as $\dot{\nu} \leq (1+\nu)(\| \mathcal{H}_1 \| + \| \mathcal{H}_2 \| \nu + \vartheta_{\sup})$. $\xi(t, \xi_0)$ is assumed to be the solution of $\dot{\xi} = (1+\xi)(\| \mathcal{H}_1 \| + \| \mathcal{H}_2 \| \xi + \vartheta_{\sup})$ and $\xi(0, \xi_0) = \xi_0$. On the basis of the aforementioned discussions, it is concluded that $\nu \leq \xi(t, \xi_0)$. Suppose that $e_y(t)$ and $\xi_0$ are equal to 0 at the initial time. Then, the smallest time interval can be acquired by integrating both sides of

$$dt = \frac{d\xi}{(1+\xi)\big(\| \mathcal{H}_1 \| + \| \mathcal{H}_2 \| \xi + \vartheta_{\sup}\big)}. \tag{29}$$

Then, it has

$$\begin{aligned} \varepsilon = &\frac{1}{\| \mathcal{H}_1 \| + \| \mathcal{H}_2 \| \xi + \vartheta_{\sup}} \\ &\times \ln\left[\frac{(\| \mathcal{H}_1 \| + \vartheta_{\sup})\xi(t, 0) + \| \mathcal{H}_1 \| + \vartheta_{\sup}}{\| \mathcal{H}_2 \| \xi(t, 0) + \| \mathcal{H}_1 \| + \vartheta_{\sup}}\right]. \end{aligned} \tag{30}$$

Set $\xi(t^*, 0) = (((\sum_{i=1}^N(\bar{\sigma}_i))/N))^{1/2}$. We have the smallest time interval

$$\begin{aligned} \triangle\bar{t} = &\frac{1}{\| \mathcal{H}_1 \| + \| \mathcal{H}_2 \| \xi + \vartheta_{\sup}} \\ &\times \ln\left[\frac{(\| \mathcal{H}_1 \| + \vartheta_{\sup})\xi(t^*, 0) + \| \mathcal{H}_1 \| + \vartheta_{\sup}}{\| \mathcal{H}_2 \| \xi(t^*, 0) + \| \mathcal{H}_1 \| + \vartheta_{\sup}}\right]. \end{aligned} \tag{31}$$

Since $\mathcal{H}_1 = \bar{A} + (1/2)\mathcal{H}_2$, $0 < \vartheta_{\sup} < +\infty$, it follows $0 < \triangle\bar{t} < \triangle t_\kappa \leq t^i_{\epsilon+1} - t^i_\epsilon$. Letting $\upsilon_i = \triangle\bar{t}$ and utilizing the aforesaid analysis yield that $\mathbb{T}_i + \upsilon_i < t^i_\epsilon + \triangle t_\kappa \leq t^{i+1}_\epsilon$. Then, one has $\mathbb{T}_i - \upsilon_i < t^{i+1}_\epsilon \leq \mathbb{T}_i$. Consequently, for $t \in \bigcup_{n\in\mathcal{N}}[n\mathcal{T}, n\mathcal{T}+\varsigma)$, the Zeno behavior is excluded. For $t \in \bigcup_{n\in\mathcal{N}}[n\mathcal{T}+\varsigma, (n+1)\mathcal{T})$, adopting the similar analysis method

above follows that the Zeno behavior can be avoided. Then, one can conclude the Zeno behavior in the proposed ETM can be excluded. That ends the proof. ■

Sufficient conditions that guarantee the exponential stability of the error system in (13) are obtained in Theorem 1. Next, we will design the controller gain $K$ and the observer gain $H$ based on Theorem 1.

*Theorem 2:* For given scalars $\mathcal{T}$, $\varsigma$, $\bar{\sigma}_i \in (0,1)$, $\varrho_\iota$ ($\iota = \{1,2\}$), the error system in (13) is exponentially stable if there exist matrices $\bar{P}_1 > 0$, $\bar{P}_2 > 0$, $\Phi_i > 0$ ($i \in \mathcal{G}$) and $\bar{Y}_1$, $\bar{Y}_2$ such that (16) and the following linear matrix inequalities hold:

$$\hat{\Upsilon}_1 = \begin{bmatrix} \hat{\Xi}^1_{11} & * & * & * \\ \bar{E}^T\bar{P}_1 & \hat{\Xi}^1_{22} & * & * \\ \hat{\Xi}^1_{31} & 0 & \hat{\Xi}^1_{33} & * \\ 0 & \bar{P}_2 & 0 & -\gamma^2 I \end{bmatrix} < 0 \tag{32}$$

$$\hat{\Upsilon}_2 = \begin{bmatrix} \hat{\Xi}^2_{11} & * & * \\ \bar{E}^T\bar{P}_1 & \hat{\Xi}^2_{22} & * \\ 0 & \bar{P}_2 & -\gamma^2 I \end{bmatrix} < 0 \tag{33}$$

where

$$\begin{aligned}
\hat{\Xi}^1_{11} &= \bar{P}_1\bar{A} + \bar{A}^T\bar{P}_1 - L_1\bar{Y}_1\bar{C}_1 - \bar{C}_1^T\bar{Y}_1^T L_1^T \\
&\quad + \bar{C}_1^T L_2^T \bar{\sigma}\Phi L_2\bar{C}_1 + \varrho_1\bar{P}_1 + \bar{D}^T\bar{D} \\
\hat{\Xi}^1_{22} &= \bar{Y}_2\bar{C}_1\bar{E} + \bar{E}^T\bar{C}_1^T\bar{Y}_2^T + \varrho_1\bar{P}_2 \\
\hat{\Xi}^1_{31} &= -2\bar{C}_1^T\bar{Y}_1^T L_1^T + \bar{C}_1^T L_2^T\bar{\sigma}\Phi L_2\bar{C}_1 \\
\hat{\Xi}^1_{33} &= -\bar{C}_1^T\Phi\bar{C}_1 + \bar{C}_1^T L_2^T\bar{\sigma}\Phi L_2\bar{C}_1 \\
\hat{\Xi}^2_{11} &= \bar{P}_1\bar{A} + \bar{A}^T\bar{P}_1 - \varrho_2\bar{P}_1 + \bar{D}^T\bar{D} \\
\hat{\Xi}^2_{22} &= \bar{Y}_2\bar{C}_1\bar{E} + \bar{E}^T\bar{C}_1^T\bar{Y}_2^T - \varrho_2\bar{P}_2.
\end{aligned}$$

Furthermore, the controller gain $K$ and observer gain $H$ are designed as

$$K = B^T P_1^{-1} Y_1,\ H = C_2^{-1} P_2^{-1} Y_2. \tag{34}$$

*Proof:* Define $\bar{P} = \begin{bmatrix} \bar{P}_1 & 0 \\ 0 & \bar{P}_2 \end{bmatrix}$ with $\bar{P}_1 = I_N \otimes P_1$, $\bar{P}_2 = I_N \otimes P_2$, $P_1 \in \mathbb{R}^6$, and $P_2 \in \mathbb{R}^3$, and $Y_1 = P_1 B K$, $Y_2 = P_2 C_2 H$, $\bar{Y}_1 = I_N \otimes Y_1$, $\bar{Y}_2 = I_N \otimes Y_2$. Then, we can obtain (32) holds. Similarly, it is easy to acquire (33) holds. Additionally, the parameters of the controller and the observer can be obtained by solving the linear matrix inequalities (32) and (33). That ends the proof. ■

## IV. Simulation Examples

A simulation example is provided to demonstrate the validity of the proposed method. Consider a multi-UAV system with five UAVs and a virtual leader. In fact, more UAVs may be required in practical applications. A large number of UAVs will lead to more computational burden. Due to the page limitation, we only take the five-follower UAV system as an example in this simulation. The case of more UAVs can be discussed and simulated in the same way.

Fig. 3 shows the directed communication topology of the five-follower UAV system, in which the 0th UAV is the virtual leader. It follows from Fig. 3 that $B_0 = \text{diag}\{1,0,0,1,1\}$, and

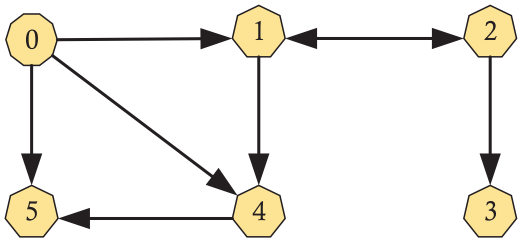


Fig. 3. Directed communication topology of the multi-UAV system.

the corresponding Laplacian matrix is given by:

$$\mathbb{L} = \begin{bmatrix} 1 & -1 & 0 & 0 & 0 \\ -1 & 1 & 0 & 0 & 0 \\ 0 & -1 & 1 & 0 & 0 \\ -1 & 0 & 0 & 1 & 0 \\ 0 & 0 & 0 & -1 & 1 \end{bmatrix}.$$

Set $C_1 = I_6$, $C_2 = I_3$, $D = I_6$, $\bar{\sigma}_1 = 0.01$, $\bar{\sigma}_2 = 0.025$, $\bar{\sigma}_3 = 0.02$, $\bar{\sigma}_4 = 0.015$, $\bar{\sigma}_5 = 0.012$, $\gamma = 3.16$. The deception attacks $f_i(t) = \mathbf{f}_i e^{-t}\sin(t)$ with $\mathbf{f}_1 = [-1.8\ 2\ -3.7]^T$, $\mathbf{f}_2 = [0.8\ 1.5\ -2.2]^T$, $\mathbf{f}_3 = [2.5\ -0.5\ 1.7]^T$, $\mathbf{f}_4 = [-1.2\ 2.2\ -0.7]^T$, $\mathbf{f}_5 = [1.2\ 2.5\ -2.6]^T$ ($i = 1,2,3,4,5$).

Choose $\mathcal{T} = 4$ s, $\varsigma = 3.4$ s, $\alpha_1 = 0.5$, $\alpha_2 = 2.8$. From Theorem 2, one can obtain the following parameters:

$$K = \begin{bmatrix} K_1 & K_2 \end{bmatrix},\quad H = \begin{bmatrix} 0_{3\times 3} & H_1 \end{bmatrix}$$

$$K_1 = \begin{bmatrix} 6.0954 & -0.0110 & -1.6860 \\ -0.0110 & 7.1812 & 0.0030 \\ -1.6860 & 0.0030 & 8.6118 \end{bmatrix}$$

$$K_2 = \begin{bmatrix} 2.8501 & -0.0105 & -1.7678 \\ -0.0105 & 3.5324 & 0.0054 \\ -1.7678 & 0.0054 & 5.4886 \end{bmatrix}$$

$$H_1 = \begin{bmatrix} -6.7614 & -0.0141 & -7.6719 \\ -12.0337 & -7.5690 & -6.0017 \\ -120.2969 & 0.1565 & -60.0403 \end{bmatrix}$$

$$\Phi_{\mathbf{c}} = \begin{bmatrix} \Phi_{\mathbf{c}1} & \Phi_{\mathbf{c}2} \end{bmatrix},\quad \mathbf{c} = 1,2,4,5$$

$$\Phi_3 = 1.0e+03 * \begin{bmatrix} \Phi_{31} & \Phi_{32} \end{bmatrix}$$

$$\Phi_{11} = \begin{bmatrix} 895.7283 & 0.0179 & 8.2544 \\ 0.0179 & 905.1892 & -0.0881 \\ 8.2544 & -0.0881 & 883.4087 \\ 119.4079 & -0.1601 & -25.0240 \\ -0.1601 & 133.9334 & 0.0522 \\ -25.0240 & 0.0522 & 156.7577 \end{bmatrix}$$

$$\Phi_{12} = \begin{bmatrix} 119.4079 & -0.1601 & -25.0240 \\ -0.1601 & 133.9334 & 0.0522 \\ -25.0240 & 0.0522 & 156.7577 \\ 492.7299 & -0.1794 & -28.8910 \\ -0.1794 & 507.2684 & 0.0714 \\ -28.8910 & 0.0714 & 535.8513 \end{bmatrix}$$

$$\Phi_{21} = \begin{bmatrix} 621.0524 & -0.0044 & 2.7849 \\ -0.0044 & 628.5009 & -0.0509 \\ 2.7849 & -0.0509 & 616.8962 \\ 60.5698 & -0.0895 & -13.8955 \\ -0.0895 & 68.8655 & 0.0279 \\ -13.8955 & 0.0279 & 81.3097 \end{bmatrix}$$

TABLE I
INITIAL VALUES OF EACH UAV

| | $(\zeta_{xi}, \zeta_{yi}, \zeta_{zi})$, m | $V_i(t)$, m/s | $\delta_i(t)$, rad | $\alpha_i(t)$, rad | $\chi_i(t)$, rad | $\beta_i(t)$, rad | $s_i$, m |
|---|---|---|---|---|---|---|---|
| UAV 1 | (9,8,83) | 45 | 0 | $\pi/3$ | $-\pi/6$ | $\pi/2$ | 20 |
| UAV 2 | (10,10,73) | 40 | 0 | $\pi/2$ | $-\pi/4$ | $-\pi/2$ | $20\sqrt{2}$ |
| UAV 3 | (20,30,113) | 46 | 0 | $-\pi/2$ | $\pi/6$ | 0 | 20 |
| UAV 4 | (24,27,102) | 46 | 0 | 0 | $\pi/2$ | $\pi$ | $20\sqrt{2}$ |
| UAV 5 | (22,25,100) | 46 | 0 | $-\pi/3$ | $\pi/4$ | $-\pi/4$ | 20 |

$$\Phi_{22} = \begin{bmatrix} 60.5698 & -0.0895 & -13.8955 \\ -0.0895 & 68.8655 & 0.0279 \\ -13.8955 & 0.0279 & 81.3097 \\ 423.4148 & -0.0698 & -11.6798 \\ -0.0698 & 428.1814 & 0.0344 \\ -11.6798 & 0.0344 & 440.8475 \end{bmatrix}$$

$$\Phi_{31} = \begin{bmatrix} 1.3147 & 0.0001 & 0.0229 \\ 0.0001 & 1.3241 & -0.0002 \\ 0.0229 & -0.0002 & 1.2805 \\ 0.2281 & -0.0003 & -0.0426 \\ -0.0003 & 0.2522 & 0.0001 \\ -0.0426 & 0.0001 & 0.2916 \end{bmatrix}$$

$$\Phi_{32} = \begin{bmatrix} 0.2281 & -0.0003 & -0.0426 \\ -0.0003 & 0.2522 & 0.0001 \\ -0.0426 & 0.0001 & 0.2916 \\ 0.5231 & -0.0004 & -0.0617 \\ -0.0004 & 0.5579 & 0.0001 \\ -0.0617 & 0.0001 & 0.6152 \end{bmatrix}$$

$$\Phi_{41} = \begin{bmatrix} 839.6489 & 0.0138 & 7.7279 \\ 0.0138 & 849.6866 & -0.0884 \\ 7.7279 & -0.0884 & 828.1151 \\ 115.5706 & -0.1543 & -24.1378 \\ -0.1543 & 129.5365 & 0.0506 \\ -24.1378 & 0.0506 & 151.5976 \end{bmatrix}$$

$$\Phi_{42} = \begin{bmatrix} 115.5706 & -0.1543 & -24.1378 \\ -0.1543 & 129.5365 & 0.0506 \\ -24.1378 & 0.0506 & 151.5976 \\ 450.4256 & -0.1725 & -27.7965 \\ -0.1725 & 464.3964 & 0.0688 \\ -27.7965 & 0.0688 & 491.9134 \end{bmatrix}$$

$$\Phi_{51} = \begin{bmatrix} 817.3904 & 0.0119 & 7.1867 \\ 0.0119 & 827.1258 & -0.0842 \\ 7.1867 & -0.0842 & 806.6644 \\ 111.1947 & -0.1479 & -23.2016 \\ -0.1479 & 124.4321 & 0.0496 \\ -23.2016 & 0.0496 & 145.8245 \end{bmatrix}$$

$$\Phi_{52} = \begin{bmatrix} 111.1947 & -0.1479 & -23.2016 \\ -0.1479 & 124.4321 & 0.0496 \\ -23.2016 & 0.0496 & 145.8245 \\ 443.1144 & -0.1605 & -25.9920 \\ -0.1605 & 455.8415 & 0.0660 \\ -25.9920 & 0.0660 & 481.9089 \end{bmatrix}.$$

Table I gives the parameters of five UAVs. Assume the leader of the UAV system with the following initial parameters [20]: The position (8, 8, 100) m, the speed (described as $40 + t$ m/s) and $\delta_0(t) = 0$ rad, $\alpha_0(t) = 0.25\pi + 0.3t$ rad, and the initial conditions of each observer are chosen as $\xi_{10} = 0$, $\xi_{20} = 0$, $\xi_{30} = 0$, $\xi_{40} = 0$, and $\xi_{50} = 0$. Based on the obtained parameters above, one can get the responses of the multi-UAV system shown in Figs. 4–13.

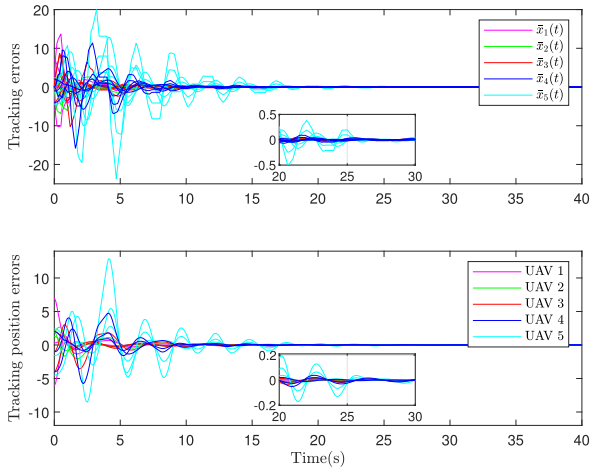


Fig. 4. Tracking errors $\bar{x}(t)$ and tracking position errors of five UAVs.

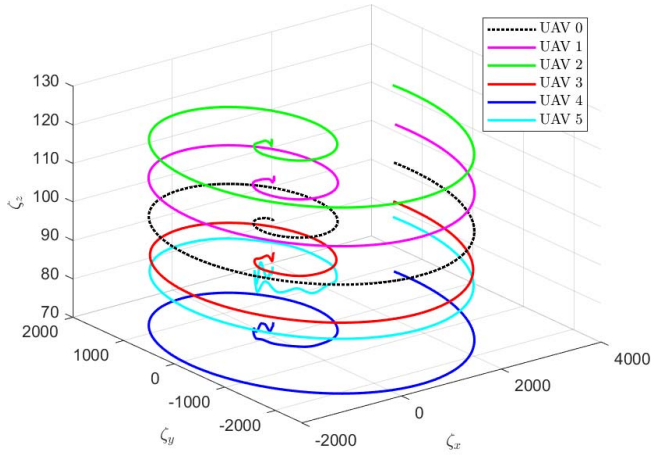


Fig. 5. Trajectories of five UAVs.

Fig. 4 shows the tracking errors $\bar{x}(t)$ and the tracking position errors of five UAVs, from which one can see that the UAV system with deception attacks is asymptotically stable. Five UAVs reach their own corresponding desired position and formulate this formation. To clearly see the respective tracking performances, we plot the tracking trajectories in Figs. 5 and 6

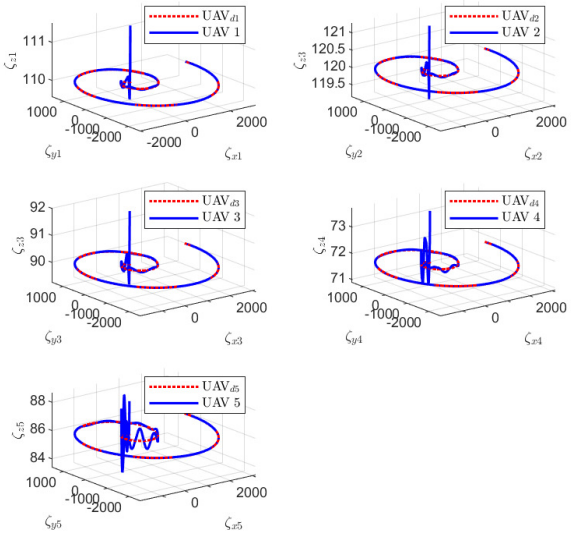


Fig. 6. Tracking trajectories of five UAVs.

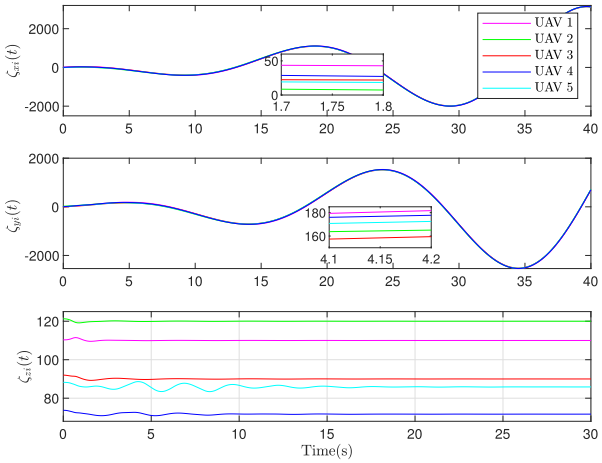


Fig. 7. Position responses of five UAVs in triaxial direction.

and the position responses in triaxial direction in Fig. 7 for each UAV. From Figs. 5–7, one can conclude that the UAV system achieves the desired formation, and each UAV keeps flying at a fixed altitude with $\zeta_{z1} = 110$ m, $\zeta_{z2} = 120$ m, $\zeta_{z3} = 90$ m, $\zeta_{z4} = 71.72$ m, and $\zeta_{z5} = 85.86$ m.

Fig. 8 shows the deception attack signals and their estimations, from which one can see that the attack observer brings the satisfactory performance of multi-UAV systems under a directed graph.

Fig. 9 presents $\sigma_i(t)$ of the proposed ETM, which finally converges to a constant after the system tends to be stable. Figs. 10 and 11 exhibit the triggering instants and releasing intervals of the proposed ETM, from which one can know that the proposed ETM discard unnecessary system output signals, thereby reducing the amount of transmitted data and alleviating the bandwidth load of the communication network. The amount of transmitted data packets is listed in Table II.

Fig. 12 shows the responses of the intermittent control $u_c^i(t)$ $(i = 1, 2, 3, 4, 5)$ with $\mathcal{T} = 4$ s, $\varsigma = 3.4$ s. It can be observed that the interval $[4, 7.4)$ s is active for the intermittent control;

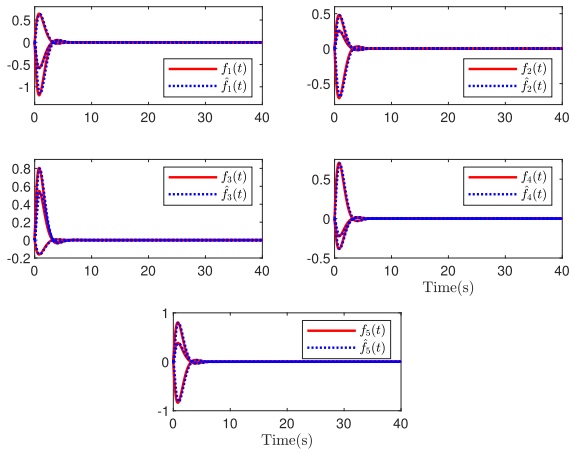


Fig. 8. Actual attacks and their estimations of five UAVs.

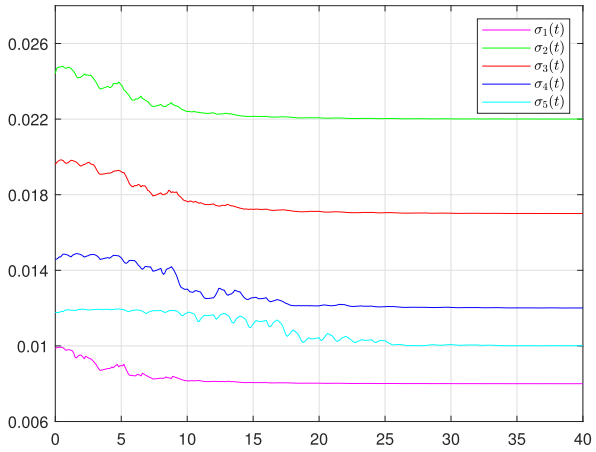


Fig. 9. $\sigma_i(t)$ of the proposed ETM.

while the intervals $[3.4, 4)$ and $[7.4, 8)$ s are the rest time of the intermittent control, during which $u_c^i(t) = 0$. This indicates that intermittent control can lighten the consumption of limited computation and energy resources. Fig. 13 displays the responses of the real control $\hbar_1(t), \ldots, \hbar_5(t)$ for five UAVs.

To further verify the superiority of the intermittent control and the ETM in (9), we present the following comparisons from the perspective of the control cost (CC) and the amount of data transmission (ADT).

First, a comparison between our proposed intermittent controller and the continuous controller in [20] is made. To describe the CC, we define the CC function for the $i$th UAV in time interval $[0, T]$ s $(T > 0)$ as

$$\mathcal{J}_i = \int_0^T \|u_c^i(t)\| dt. \tag{35}$$

In the following, the CC function will be used to evaluate the CC of the system with two different types of controllers under the same condition and parameters as above. The inputs of a continuous controller in [20] for five UAVs are shown in Fig. 14. From Figs. 12 and 14, one knows that a larger control effort is required by using our control approach compared to the continuous controller in [20]. Over the simulation time

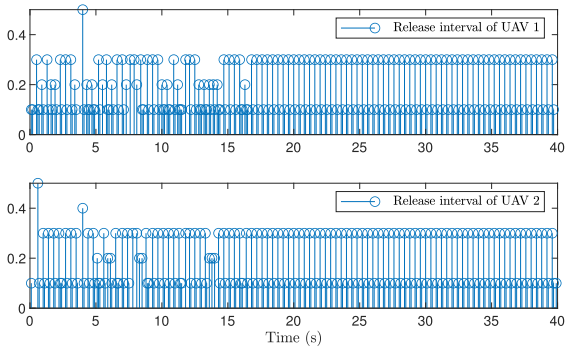


Fig. 10. Release instants and release intervals of UAVs 1 and 2.

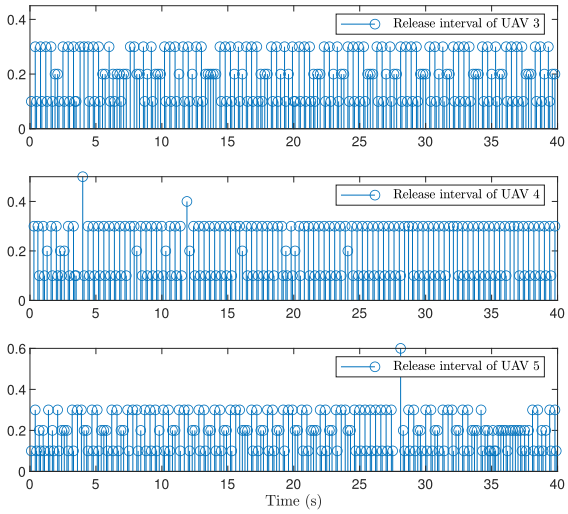


Fig. 11. Release instants and release intervals of UAVs 3–5.

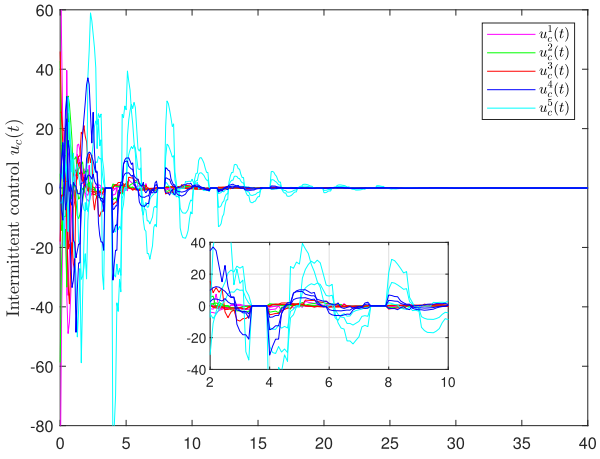


Fig. 12. Intermittent control with $\mathcal{T} = 4$ s, $\varsigma = 3.4$ s for five UAVs.

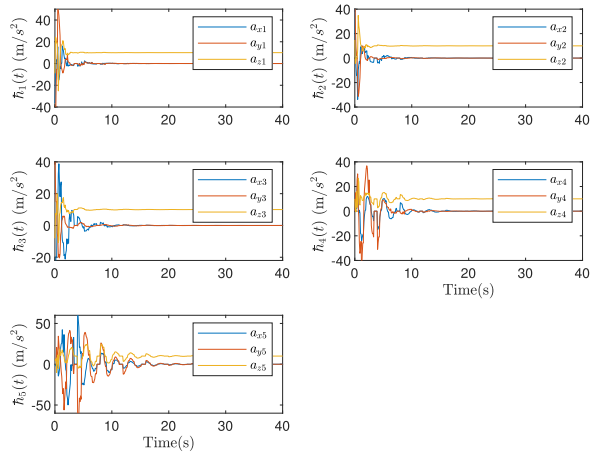


Fig. 13. Real control of five UAVs.

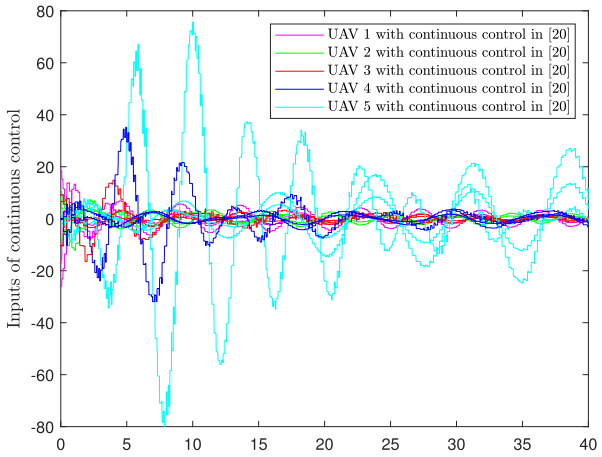


Fig. 14. Inputs of continuous control in [20] for five UAVs.

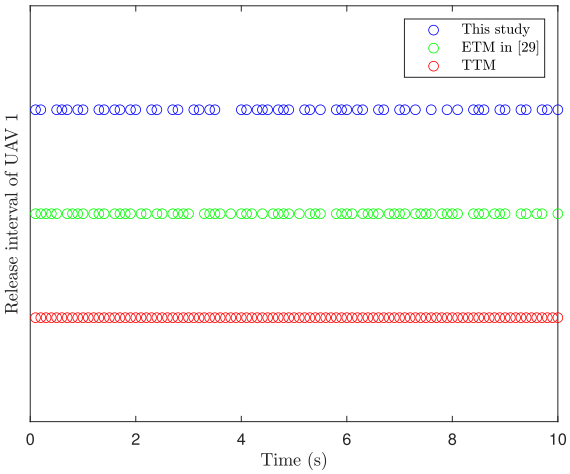


Fig. 15. Release instants and release intervals of UAV 1 under three communication mechanisms.

interval $[0, 40]$ s, the CC of five UAVs for two controllers is calculated in Table III.

From Table III, one can see that the CC by using our proposed intermittent control strategy was reduced by 71.99% compared to the one under the traditional continuous controller in [20]. This illustrates that our proposed control strategy has the advantage of mitigating the consumption of computation and energy resources, which is an important performance index for UAV systems.

To show the performance of the proposed ETM, we present releasing instants and intervals for five UAVs using the time-triggered mechanism (TTM), the ETM in [29] without

TABLE II
ADT OF FIVE UAVS IN 40 S

| | TTM | ETM in [29] | This study |
|---|---|---|---|
| ADT of UAV 1 | 400 | 255 | 198 |
| ADT of UAV 2 | 400 | 238 | 186 |
| ADT of UAV 3 | 400 | 237 | 185 |
| ADT of UAV 4 | 400 | 224 | 178 |
| ADT of UAV 5 | 400 | 239 | 188 |

TABLE III
CC FOR FIVE UAVS OVER [0, 40] S

| | Continuous controller in [20] | Intermittent controller in this study |
|---|---|---|
| UAV 1 | 4.5829e+04 | 1.3516e+04 |
| UAV 2 | 3.8447e+04 | 1.0195e+04 |
| UAV 3 | 4.4683e+04 | 1.0354e+04 |
| UAV 4 | 4.0784e+04 | 1.0416e+04 |
| UAV 5 | 2.0949e+04 | 8.9206e+03 |
| Total | 1.9069e+05 | 5.3402e+04 |

an average method, and our proposed ETM. In the TTM and the ETM in [29], the sampling period is 0.1 s. The comparative results of UAV 1 over [0, 10] s are shown in Fig. 15, and other UAVs have similar results which are omitted here. Besides, Table II displays the ADT of five UAVs under the above communication mechanisms in 40 s.

As shown in Table II and Fig. 15, the ADT under our proposed ETM is evidently less than the one under the TTM and the ETM in [29], which reveals that our proposed ETM is more effective than other triggering mechanisms in reducing the amount of redundant data.

## V. CONCLUSION

In this article, the event-based formation problem of multi-UAV systems with directed graphs and deception attacks has been studied by using an intermittent control scheme. Different from the available research on multi-UAV systems with continuous control strategy, the intermittent control scheme effectively saves computation resources. The ETM using the average method is developed to reduce the amount of unexpected triggered events, thus relieving the bandwidth burden of the communication network. By considering deception attacks, an overall error system, containing a tracking error and an attack estimation error, has been constructed based on the Kronecker product. Moreover, sufficient conditions for the multi-UAV system to achieve the formation are obtained. Finally, the validity of the proposed theoretical results for five UAVs is demonstrated via a simulation example. The future work will be concerned with the problem of the formation control for multi-UAV systems with multiple leaders, along with fault detection, and the isolation of the cyber-attacks.

## REFERENCES

[1] Z. Peng, J. Wang, and D. Wang, "Distributed maneuvering of autonomous surface vehicles based on neurodynamic optimization and fuzzy approximation," *IEEE Trans. Control Syst. Technol.*, vol. 26, no. 3, pp. 1083–1090, May 2018.

[2] X. Dong, Y. Zhou, Z. Ren, and Y. Zhong, "Time-varying formation tracking for second-order multi-agent systems subjected to switching topologies with application to quadrotor formation flying," *IEEE Trans. Ind. Electron.*, vol. 64, no. 6, pp. 5014–5024, Jun. 2017.

[3] Z. Gu, T. Yin, and Z. Ding, "Path tracking control of autonomous vehicles subject to deception attacks via a learning-based event-triggered mechanism," *IEEE Trans. Neural Netw. Learn. Syst.*, vol. 32, no. 12, pp. 5644–5653, Dec. 2021.

[4] J. Ye, C. Fu, F. Lin, F. Ding, S. An, and G. Lu, "Multi-regularized correlation filter for UAV tracking and self-localization," *IEEE Trans. Ind. Electron.*, vol. 69, no. 6, pp. 6004–6014, Jun. 2022.

[5] X. Tian, J. Shao, D. Ouyang, and H. T. Shen, "UAV-satellite view synthesis for cross-view geo-localization," *IEEE Trans. Circuits Syst. Video Technol.*, vol. 32, no. 7, pp. 4804–4815, Jul. 2022.

[6] H. Liu, Q. Chen, N. Pan, Y. Sun, Y. An, and D. Pan, "UAV stocktaking task-planning for industrial warehouses based on the improved hybrid differential evolution algorithm," *IEEE Trans. Ind. Informat.*, vol. 18, no. 1, pp. 582–591, Jan. 2022.

[7] J. Wang, L. Han, X. Dong, Q. Li, and Z. Ren, "Distributed sliding mode control for time-varying formation tracking of multi-UAV system with a dynamic leader," *Aerosp. Sci. Technol.*, vol. 111, Apr. 2021, Art. no. 106549.

[8] K. Guo, X. Li, and L. Xie, "Ultra-wideband and odometry-based cooperative relative localization with application to multi-UAV formation control," *IEEE Trans. Cybern.*, vol. 50, no. 6, pp. 2590–2603, Jun. 2020.

[9] G. Shao, Y. Ma, R. Malekian, X. Yan, and Z. Li, "A novel cooperative platform design for coupled USV–UAV systems," *IEEE Trans. Ind. Informat.*, vol. 15, no. 9, pp. 4913–4922, Sep. 2019.

[10] J. Chen et al., "Joint task assignment and spectrum allocation in heterogeneous UAV communication networks: A coalition formation game-theoretic approach," *IEEE Trans. Wireless Commun.*, vol. 20, no. 1, pp. 440–452, Jan. 2021.

[11] Z. Yu et al., "Distributed adaptive fault-tolerant close formation flight control of multiple trailing fixed-wing UAVs," *ISA Trans.*, vol. 106, pp. 181–199, Nov. 2020.

[12] H. Su, J. Zhang, and X. Chen, "A stochastic sampling mechanism for time-varying formation of multiagent systems with multiple leaders and communication delays," *IEEE Trans. Neural Netw. Learn. Syst.*, vol. 30, no. 12, pp. 3699–3707, Dec. 2019.

[13] N. Nagarani, P. Venkatakrishnan, and N. Balaji, "Unmanned aerial vehicle's runway landing system with efficient target detection by using morphological fusion for military surveillance system," *Comput. Commun.*, vol. 151, pp. 463–472, Feb. 2020.

[14] J. Zhang, J. Yan, and P. Zhang, "Multi-UAV formation control based on a novel back-stepping approach," *IEEE Trans. Veh. Technol.*, vol. 69, no. 3, pp. 2437–2448, Mar. 2020.

[15] X. Dong, B. Yu, Z. Shi, and Y. Zhong, "Time-varying formation control for unmanned aerial vehicles: Theories and applications," *IEEE Trans. Control Syst. Technol.*, vol. 23, no. 1, pp. 340–348, Jan. 2015.

[16] S. Zhao, X. Wang, Z. Lin, D. Zhang, and L. Shen, "Integrating vector field approach and input-to-state stability curved path following for unmanned aerial vehicles," *IEEE Trans. Syst., Man, Cybern., Syst.*, vol. 50, no. 8, pp. 2897–2904, Aug. 2020.

[17] Z. Zuo, B. Tian, M. Defoort, and Z. Ding, "Fixed-time consensus tracking for multiagent systems with high-order integrator dynamics," *IEEE Trans. Autom. Control*, vol. 63, no. 2, pp. 563–570, Feb. 2018.

[18] W. Zhu, W. Cao, and Z.-P. Jiang, "Distributed event-triggered formation control of multiagent systems via complex-valued Laplacian," *IEEE Trans. Cybern.*, vol. 51, no. 4, pp. 2178–2187, Apr. 2021.

[19] Y.-B. Bae, Y.-H. Lim, and H.-S. Ahn, "Distributed robust adaptive gradient controller in distance-based formation control with exogenous disturbance," *IEEE Trans. Autom. Control*, vol. 66, no. 6, pp. 2868–2874, Jun. 2021.

[20] L. Wei, M. Chen, and T. Li, "Dynamic event-triggered cooperative formation control for UAVs subject to time-varying disturbances," *IET Control Theory Appl.*, vol. 14, no. 17, pp. 2514–2525, Nov. 2020.

[21] Y. Wang, D. Wang, and S. Zhu, "Cooperative moving path following for multiple fixed-wing unmanned aerial vehicles with speed constraints," *Automatica*, vol. 100, pp. 82–89, Feb. 2019.

[22] D. M. Stipanovic, G. Inalhan, R. Teo, and C. J. Tomlin, "Decentralized overlapping control of a formation of unmanned aerial vehicles," *Automatica*, vol. 40, no. 8, pp. 1285–1296, Aug. 2004.

[23] X. Liu and T. Chen, "Synchronization of complex networks via aperiodically intermittent pinning control," *IEEE Trans. Autom. Control*, vol. 60, no. 12, pp. 3316–3321, Dec. 2015.

[24] P. Wang, Y. Hong, and H. Su, "Stabilization of stochastic complex-valued coupled delayed systems with Markovian switching via periodically intermittent control," *Nonlinear Anal. Hybrid Syst.*, vol. 29, pp. 395–413, Aug. 2018.

[25] D. Ouyang, J. Shao, H. Jiang, S. K. Nguang, and H. T. Shen, "Impulsive synchronization of coupled delayed neural networks with actuator saturation and its application to image encryption," *Neural Netw.*, vol. 128, pp. 158–171, Aug. 2020.

[26] F. Qu, E. Tian, and X. Zhao, "Chance-constrained $H_\infty$-infinity state estimation for recursive neural networks under deception attacks and energy constraints: The finite-horizon case," *IEEE Trans. Neural Netw. Learn. Syst.*, to be published, doi: 10.1109/TNNLS.2021.3137426.

[27] D. Yue, E. Tian, and Q.-L. Han, "A delay system method for designing event-triggered controllers of networked control systems," *IEEE Trans. Autom. Control*, vol. 58, no. 2, pp. 475–481, Feb. 2013.

[28] Z. Gu, C. K. Ahn, D. Yue, and X. Xie, "Event-triggered $H_\infty$ filtering for T–S fuzzy-model-based nonlinear networked systems with multi-sensors against DoS attacks," *IEEE Trans. Cybern.*, vol. 52, no. 6, pp. 5311–5321, Jun. 2022.

[29] S. Yan, M. Shen, S. K. Nguang, and G. Zhang, "Event-triggered $H_\infty$ control of networked control systems with distributed transmission delay," *IEEE Trans. Autom. Control*, vol. 65, no. 10, pp. 4295–4301, Oct. 2020.

[30] X. Xie, Q. Zhou, D. Yue, and H. Li, "Relaxed control design of discrete-time Takagi–Sugeno fuzzy systems: An event-triggered real-time scheduling approach," *IEEE Trans. Syst., Man, Cybern., Syst.*, vol. 48, no. 12, pp. 2251–2262, Dec. 2018.

[31] X. Xie, D. Yue, J. H. Park, and J. Liu, "Enhanced stabilization of discrete-time Takagi–Sugeno fuzzy systems based on a comprehensive real-time scheduling model," *IEEE Trans. Syst., Man, Cybern., Syst.*, vol. 52, no. 2, pp. 881–892, Feb. 2022.

[32] L. Zhang, S. K. Nguang, D. Ouyang, and S. Yan, "Synchronization of delayed neural networks via integral-based event-triggered scheme," *IEEE Trans. Neural Netw. Learn. Syst.*, vol. 31, no. 12, pp. 5092–5102, Dec. 2020.

[33] X. Sun, Z. Gu, D. Yue, and X. Xie, "Event-triggered $H_\infty$ filtering for cyber-physical systems against DoS attacks," *IEEE Trans. Syst. Man, Cybern., Syst.*, early access, Nov. 8, 2022, doi: 10.1109/TSMC.2022.3218023.

[34] J. Liu, Y. Gu, X. Xie, D. Yue, and J. H. Park, "Hybrid-driven-based $H_\infty$ control for networked cascade control systems with actuator saturations and stochastic cyber attacks," *IEEE Trans. Syst. Man, Cybern., Syst.*, vol. 49, no. 12, pp. 2452–2463, Dec. 2019.

[35] Z. Gu, P. Shi, D. Yue, and Z. Ding, "Decentralized adaptive event-triggered $H_\infty$ filtering for a class of networked nonlinear interconnected systems," *IEEE Trans. Cybern.*, vol. 49, no. 5, pp. 1570–1579, May 2019.

[36] E. Tian and C. Peng, "Memory-based event-triggering $H_\infty$ load frequency control for power systems under deception attacks," *IEEE Trans. Cybern.*, vol. 50, no. 11, pp. 4610–4618, Nov. 2020.

[37] Z. Gu, C. K. Ahn, S. Yan, X. Xie, and D. Yue, "Event-triggered filter design based on average measurement output for networked unmanned surface vehicles," *IEEE Trans. Circuits Syst. II, Exp. Briefs*, vol. 69, no. 9, pp. 3804–3808, Sep. 2022.

[38] X. Sun, Z. Gu, F. Yang, and S. Yan, "Memory-event-trigger-based secure control of cloud-aided active suspension systems against deception attacks," *Inf. Sci.*, vol. 543, pp. 1–17, Jan. 2021.

[39] J. Liu, T. Yin, J. Cao, D. Yue, and H. R. Karimi, "Security control for T–S fuzzy systems with adaptive event-triggered mechanism and multiple cyber-attacks," *IEEE Trans. Syst., Man, Cybern., Syst.*, vol. 51, no. 10, pp. 6544–6554, Oct. 2021.

[40] C. Peng and H. Sun, "Switching-like event-triggered control for networked control systems under malicious denial of service attacks," *IEEE Trans. Autom. Control*, vol. 65, no. 9, pp. 3943–3949, Sep. 2020.

[41] F. Han, H. Dong, Z. Wang, and G. Li, "Local design of distributed $H_\infty$ consensus filtering over sensor networks under multiplicative noises and deception attacks," *Int. J. Robust Nonlinear Control*, vol. 29, no. 8, pp. 2296–2314, May 2019.

[42] H. Rezaee and F. Abdollahi, "Motion synchronization in unmanned aircrafts formation control with communication delays," *Commun. Nonlinear Sci. Numer. Simul.*, vol. 18, no. 3, pp. 744–756, Mar. 2013.

[43] X. Liu and T. Chen, "Cluster synchronization in directed networks via intermittent pinning control," *IEEE Trans. Neural Netw. Learn. Syst.*, vol. 22, no. 7, pp. 1009–1020, Jul. 2011.

[44] P. Tabuada, "Event-triggered real-time scheduling of stabilizing control tasks," *IEEE Trans. Autom. Control*, vol. 52, no. 9, pp. 1680–1685, Sep. 2007.

[45] D. P. Borgers and W. P. M. Heemels, "Event-separation properties of event-triggered control systems," *IEEE Trans. Autom. Control*, vol. 59, no. 10, pp. 2644–2656, Oct. 2014.

**Tingting Yin** received the B.S. degree in network engineering from the Nanjing University of Posts and Telecommunications, Yangzhou, China, in 2017, and the M.S. degree in software engineering from the Nanjing University of Finance and Economics, Nanjing, China, in 2020. She is currently pursuing the Ph.D. degree with the College of Mechanical and Electronic Engineering, Nanjing Forestry University, Nanjing.

Her research interests include cyber-physical systems, multiagent systems, and T-S fuzzy systems.

**Zhou Gu** (Member, IEEE) received the B.S. degree in automation from North China Electric Power University, Beijing, China, in 1997, and the M.S. and Ph.D. degrees in control science and engineering from the Nanjing University of Aeronautics and Astronautics, Nanjing, China, in 2007 and 2010, respectively.

From September 1999 to January 2013, he was with the School of Power engineering, Nanjing Normal University, Nanjing, as an Associate Professor. He is currently a Professor with Nanjing Forestry University, Nanjing. His current research interests include networked control systems, time-delay systems, and reliable control and their applications.

**Ju H. Park** (Senior Member, IEEE) received the Ph.D. degree in electronics and electrical engineering from the Pohang University of Science and Technology (POSTECH), Pohang, South Korea, in 1997.

From May 1997 to February 2000, he was a Research Associate with the Engineering Research Center-Automation Research Center, POSTECH. He joined Yeungnam University, Gyeongsan, South Korea, in March 2000, where he is currently the Chuma Chair Professor. He has coauthored the monographs *Recent Advances in Control and Filtering of Dynamic Systems with Constrained Signals* (New York, NY, USA: Springer-Nature, 2018) and *Dynamic Systems With Time Delays: Stability and Control* (New York, NY, USA: Springer-Nature, 2019) and is an Editor of an edited volume *Recent Advances in Control Problems of Dynamical Systems and Networks* (New York: Springer-Nature, 2020). His research interests include robust control and filtering, neural/complex networks, fuzzy systems, multiagent systems, and chaotic systems. He has authored a number of articles in these areas.

Dr. Park is a fellow of the Korean Academy of Science and Technology (KAST). Since 2015, he has been a recipient of the Highly Cited Researchers Award by Clarivate Analytics (formerly, Thomson Reuters) and listed in three fields, engineering, computer sciences, and mathematics from 2019 to 2022. He also serves as an Editor of the *International Journal of Control, Automation and Systems*. He is also a Subject Editor/Advisory Editor/Associate Editor/Editorial Board Member of several international journals, including *IET Control Theory and Applications*, *Applied Mathematics and Computation*, *Journal of The Franklin Institute*, *Nonlinear Dynamics*, *Engineering Reports*, *Cogent Engineering*, IEEE TRANSACTIONS ON FUZZY SYSTEMS, IEEE TRANSACTIONS ON NEURAL NETWORKS AND LEARNING SYSTEMS, and IEEE TRANSACTIONS ON CYBERNETICS.